VOL. 21, NO. 12, JUNE 2026 ISSN 1819-6608
ARPN Journal of Engineering and Applied Sciences
©2006-2026 Asian Research Publishing Network (ARPN). All rights reserved.
www.arpnjournals.com

IMPROVED MOBILE ROBOT BASED GAS DISTRIBUTION MAPPING THROUGH AMBIENT TEMPERATURE INFORMATION FOR INDOOR ENVIRONMENT

Zaffry Hadi Mohd Juffry[1], Kamarulzaman Kamarudin[2], Abdul Hamid Adom[2], Retnam Visvanathan[3], Abdulnasser Nabil Abdullah[2], Wan Abdul Syaqur Norzam[4], Ahmad Hakimi Ahmad Sa'ahiry[5], Zairi Ismael Rizman[6] and Nasr Abdalmanan[2]

[1]Faculty of Artificial Intelligence and Cyber Security, Universiti Teknikal Malaysia Melaka, Malaysia
[2]Faculty of Electrical Engineering Technology, Universiti Malaysia Perlis, Malaysia
[3]Centre of Excellence for Advanced Sensor Technology (CEASTech), Universiti Malaysia Perlis, Malaysia
[4]School of Electrical and Electronic Engineering, Universiti Sains Malaysia, Penang, Malaysia
[5]Faculty of Information and Communication Technology, Universiti Tunku Abdul Rahman, Perak, Malaysia
[6]Faculty of Electrical Engineering, Universiti Teknologi MARA, Dungun, Terengganu, Malaysia
E-Mail: zaffry@utem.edu.my

ABSTRACT

Gas Distribution Mapping (GDM) is a method used to represent the dispersion of harmful gas and serves the purpose of localizing the gas source within an environment. Basically, a mobile robot carrying a gas sensor, known as Mobile Robot Olfaction (MRO), helps to collect important readings in the contaminated area and is used to generate the GDM. There are many environmental factors that could affect gas dispersion that were reported in previous work, which could also affect the quality of the GDM. However, one frequently neglected important environmental factor is ambient temperature, which could influence the dispersion of gas within the indoor environment. This paper aims to improve the original algorithm of GDM by incorporating ambient temperature information into the algorithm, which is known as the Temperature-compensated Kernel DM+V algorithm. A solution was proposed to improve the original Kernel DM+V algorithm by considering the ambient temperature reading within the environment. The original algorithm of GDM was modified by altering the kernel width according to the ambient temperature reading. The proposed solution was observed under both cooler and warmer environments, showing that the gas distribution in the warmer environment extended over a larger area compared with its dispersion in the cooler environment. Compared to the conventional method, it seems to represent a similar gas distribution even though there is a difference in ambient temperature level. This study demonstrates that incorporating ambient temperature information into the original GDM algorithm results in a more realistic gas distribution map that accurately reflects gas dispersion under varying environmental conditions.

Keywords: mobile olfaction, gas source localization, gas distribution mapping, ambient temperature, and indoor gas dispersion.

Manuscript Received 5 May 2026; Revised 31 May 2026; Published 20 August 2026

INTRODUCTION

With the rapid growth of industrial sectors, the use of dangerous chemical gases, such as Ammonia (NH3), Chlorine (Cl), Carbon Dioxide (CO2), and other harmful Volatile Organic Compounds (VOCs), has also risen. These gases pose significant risks to public health and safety, especially when accidental leaks occur. For instance, in 2020, an incident of harmful gas leakage occurred at a factory's storeroom in the Kulim Hi-Tech, Kedah, Malaysia. Even though no fatalities were reported, 59 individuals fell ill due to toxic ammonia inhalation [1]. The affected workers were first decontaminated to neutralize the gas before they were handed over to the hospital for further treatment. In the most recent incident of 2023, a gas leak in Punjab, India, resulted in the tragic loss of 11 lives, marking the latest fatal industrial accident in the country. The rescue team attributes this unfortunate event to the company's inadequate safety standards and insufficient checking procedures, ultimately leading to the incident [2].

These incidents underscore the urgent need for more effective gas detection and localization systems. Toxic gases are often odorless, colorless, and undetectable by the human sensory system, making them especially dangerous [3]. Prolonged exposure to such gases can cause a variety of serious health issues, including respiratory damage, neurological effects, and even death [4]. Currently, emergency responses to gas leaks involve humans localizing the source, which exposes them to potential hazards [5]. Additionally, the ability to localize gas sources quickly and accurately is essential not only for emergency response but also for applications such as air quality monitoring, environmental protection, and drug detection.

Many industries have adopted stationary gas sensor systems to detect the presence of harmful gases. These systems offer several advantages, such as providing detailed information about harmful gases in a specific environment and collecting essential data on a regular basis. However, a major limitation of stationary systems is their ability to gather gas concentration data only within a

©2006-2026 Asian Research Publishing Network (ARPN). All rights reserved.

confined area which often incurs the problems of non-detection zones and low-granularity monitoring, especially in complex indoor scenarios where environmental factors are dynamic and non-convex function [6]. Furthermore, they lack flexibility, are costly, are time-consuming to install, and remain incapable of performing gas source localization [7]. Therefore, using a mobile robot carrying a gas sensor is more practical since it is easier to deploy, can do repetitive tasks without getting exhausted, and can enter contaminated areas that human beings cannot reach. Moreover, it can also provide a higher and adaptive resolution than a stationary sensor network, further offering accurate localization and creating a better gas distribution model [8].

GDM is a process of presenting the spatial distribution of gases within the environment, providing valuable insight into the gas dispersion pattern. One of the key challenges in GDM is the unpredictable nature of harmful gas dispersion. In actual indoor gas leakage accidents, the process of gas diffusion is governed by complex mechanisms that are influenced by a variety of environmental factors, including temperature, pressure, airflow, and obstacles [9, 10]. Failure to consider these factors during the development of the GDM may lead to misinterpretations and inaccurate representations of the gas dispersion. Therefore, it is crucial to consider all relevant environmental factors to ensure the gas map accurately reflects the true dispersion of the gas.

Temperature is widely recognized as a critical environmental parameter affecting gas dispersion. A study has shown that higher ambient temperature can increase gas diffusivity and spread distance in indoor environments, indicating that temperature significantly affects the dispersion process [11]. However, there are currently no reports on the integration of temperature effects within GDM algorithms. In practical gas leakage scenarios, leaks may occur under varying ambient temperature conditions influenced by ventilation systems, external climate changes, and seasonal variations. Neglecting these temperature-related factors can lead to inaccuracies in predicting gas spread and behavior within indoor spaces.

Overall, the development of a mobile robot-based gas distribution mapping using ambient temperature information is motivated by the growing need for more effective, flexible, and accurate methods of representing harmful gas spread in indoor environments. This research proposes an enhancement to the Kernel DM+V algorithm by incorporating ambient temperature information and highlights the significant impact of considering temperature on GDM representation.

RELATED WORK

Earlier sections outlined the relevance of gas detection using mobile robots and highlighted why environmental factors should be considered while constructing GDM. More recently, GDM has attracted growing interest among researchers, expanding the role of mobile robots beyond source localization alone. As mobile robotic systems continue to advance rapidly, an increasing number of studies focusing on GDM have been published over recent years.

In the early work on GDM, [12] developed a robot capable of mapping gas distribution across a specific area. A conductive polymer sensor was mounted on a mobile robot, which conducted random walks throughout the experiment. To facilitate data interpretation, the number of ‘odor hits' (i.e., measurements exceeding a predefined threshold) was recorded and displayed as a two-dimensional (2D) histogram. However, for the robot to generate a reliable representation of the gas distribution, it needed to explore every part of the area, as no extrapolation method was proposed. Consequently, this approach is considered unsuitable for large-area applications due to the extended time required.

Later, [13] proposed a probabilistic method to cope with the extrapolation issue based on previous work proposed by [12]. This method implements a statistical approach on the grid cells to create gas concentration map data. It represents an estimation of the gas distribution mean and applies an extrapolation algorithm by convolving a single point of gas sensor reading to a nearby location (i.e., neighborhood cells) by using a symmetrical Gaussian kernel, as shown in Figure-1. Therefore, each cell on the map will have a predefined gas mean reading from all measurements. The method assumes the robot's position is known and the map is built to refer to the GDM. This approach was later extended to a three-dimensional (3D) GDM which implements a tri-variate Gaussian kernel to extrapolate the gas sensor reading at a different height [14]. A notable strength of this method is that the robot is not required to explore each part of the area to create a reliable gas distribution map. However, this method relies on a fixed-size Gaussian kernel, as it does not consider any environmental factor in the algorithm.

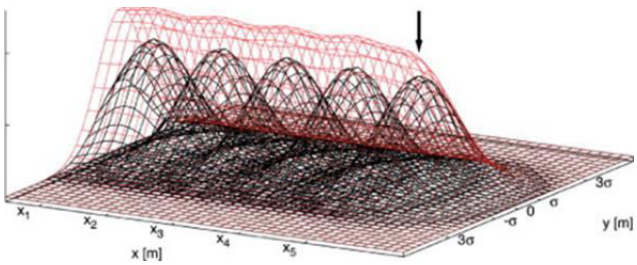


Figure-1. Sum of likelihood function Gaussian extrapolation along a straight line [13]

Then, [15] enhanced the work by proposing a method that integrates simultaneous localization and mapping (SLAM) with GDM. This method displayed the obstacles around the robot and the gas concentration in a single grid map, allowing the robot to explore an unknown environment. This work implemented the Rao-Blackwellisation particle filter to estimate the robot's position and then build the GDM while exploring the

©2006-2026 Asian Research Publishing Network (ARPN). All rights reserved.

environment. This approach enables a mobile robotic platform to construct gas distribution maps in real time by employing SLAM as the positional framework for the sequential map generation process.

Next, [16] presented a method that treated GDM as a regression problem and applied Gaussian Process Mixture (GPM), allowing GDM to precisely smooth the background signal and the area with high concentration. It also proves that the accuracy of gas source prediction can be improved by variance computation. Following this approach, the Kernel DM+V algorithm was proposed with two parallel estimation processes using mean and variance prediction of GDM [8]. The work shows that variability lies with the gas sensor measurements, making the variance map more accurate in estimating the gas source location. In addition, the larger dataset can be handled by Kernel DM+V with a more straightforward learning procedure.

Over recent years, the researchers have acknowledged the necessity of integrating environmental variables that affect gas dispersion, such as wind, obstacles, pressure, temperature, and humidity, into the GDM algorithm. Consequently, [17, 18] expanded the Kernel DM+V to 2D and 3D Kernel DM+V/W, which incorporated wind information into the algorithm. The robot is equipped with a vertical array of gas sensors and an ultrasonic anemometer to measure the environmental wind vector. This vertical array of gas sensors, along with the ultrasonic anemometer, collects wind data. The wind vector information is then utilized to modify the shape of the bivariate Gaussian kernel, as illustrated in Figure-2. The kernel's shape and positioning correlate with the nearby wind speed, enabling the algorithm to incorporate data regarding the source and probable destination of the chemical. The results of this study demonstrate an enhancement in the mapping of gas dispersion compared to earlier approaches.

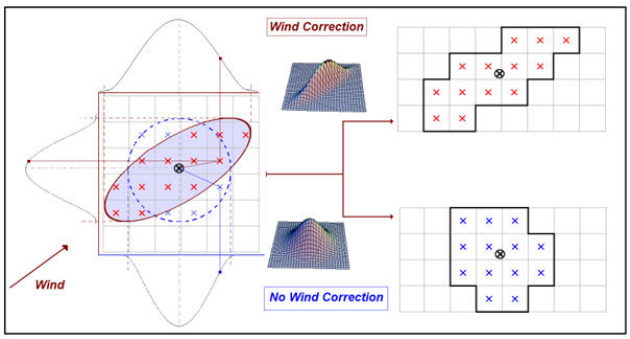


Figure-2. Gaussian kernel shape depending on the wind vector [17]

Despite these advancements, the algorithm has several drawbacks: firstly, it is time-consuming and unsuitable for emergency applications; secondly, it fails to include data obtained during movement, which, although inherently noisy, can provide valuable insights [20]: thirdly, the stretching parameter of the algorithm must be set manually or empirically [21]. In addition, the algorithm neglects the impact of airflow and inadequately differentiates between the upwind and downwind dispersion. To address this problem, a study has been conducted by [22] that enhanced the method by introducing the Kernel DM + V/W+ method. This method introduces a local airflow correction term in the Kernel DM + V method, which strengthens the influence of the concentration reading on the downwind area and weakens its influence on the upwind area.

Next, study in [23] pointed out the problem of time-variant of gas measurement that is taken at the exact location but at different instances of time. This is due to the transient nature of the gas. To solve the problem, a method called Gaussian Markov Random Field (GMRF) was presented by accounting for obstacles and the ephemeral character of gas concentration, suitable for GDM. The current gas distribution measurement is more faithful than the older one. Hence, the gas measurements at different times but at various locations will be treated by combining them according to their respective weight. The approach produces better GDM in a structured indoor environment.

Another notable study was reported in [24], which continued the work done by [8, 14], improving the performance of gas mapping using a real-time SLAM-GDM combination as shown in Figure-3. In this work, Hector SLAM was integrated with the Kernel DM+V algorithm. The researchers produced real-time gas map data that could accurately predict the gas source with a displacement error in the range of 0.5 m-1.5 m [24]. The predictions were accurate by considering the large environment being tested and taking into account the memory effect of the gas sensors.

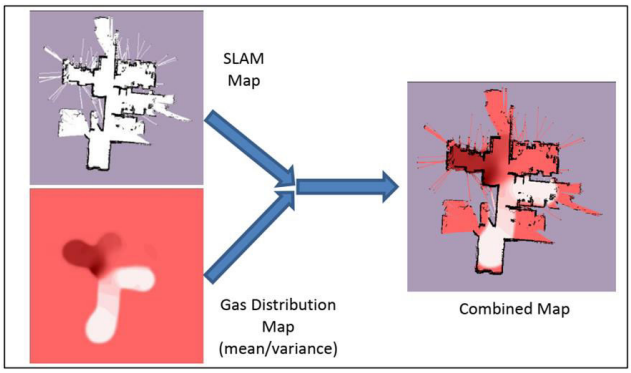


Figure-3. Combination of SLAM and GDM [23].

The advancement of the GDM algorithm continued when a study in [26] improved the system by applying propagated Distance Transform (DT) as the weighing function. The weighing function of Kernel DM+V was improved using a propagated DT (i.e., City Block) to obtain a 'true' correlation between cells if obstacles are present in between. The estimated GDM is more contained within the environment, thus providing a better estimation of gas dispersion. Figure-4 illustrates a

©2006-2026 Asian Research Publishing Network (ARPN). All rights reserved.

contrast between GDM when utilizing the DT algorithm and when not employing the DT algorithm. However, this algorithm has some drawbacks, as the computation of DT is heavy and needs to use parallel computing, such as using the Compute Unified Device Architecture (CUDA), which is only available in the Graphics Processing Unit (GPU). This will increase the computational power of the mobile robot, which will consume more power than previous methods, which could be only used by normal CPU.

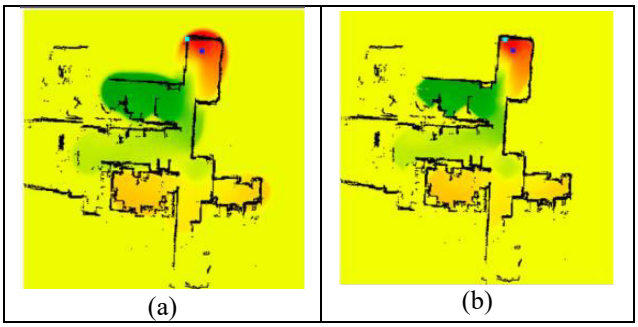


Figure-4. (a) GDM without distance propagation, and (b) GDM with distance propagation [25]

From the literature on GDM works, various environmental factors such as obstacles, wind, time-variant, building layout, and surrounding structures have been considered into the GDM algorithm. However, there is still no work on the consideration of ambient temperature information in the GDM algorithm. The author believes that the algorithm should incorporate a broader range of environmental factors influencing gas dispersion to enhance the gas dispersion model. Hence, the main contribution in this work is to incorporate ambient temperature information to improve the conventional GDM algorithm.

METHODOLOGY

This section presents the original Kernel DM+V algorithm used to calculate the gas distribution mapping, followed by the proposed Temperature-Compensated Kernel DM+V approach that incorporates ambient temperature readings. Then, the overall robot system architecture is described and concludes with the experimental setup used to generate GDM with both approaches.

Kernel DM+V Algorithm

The Kernel DM+V uses a uni-variate Gaussian weighting function N to represent the importance of measurement r_i gained from location $x^{(k)}$ across the grid cells of the map. The initial step of the Kernel DM+V formulation is to compute two temporary grid maps of the cumulative important weight, $\Omega^{(k)}$ and the cumulative weight reading, $R^{(k)}$ as shown in Equation (1) and Equation (2).

$$\Omega^{(k)} = \sum_{i=1}^{n} N\left(\left|x_i - x^{(k)}\right|, \sigma\right), \quad (1)$$

$$R^{(k)} = \sum_{i=1}^{n} N\left(\left|x_i - x^{(k)}\right|, \sigma\right).r_i \quad (2)$$

where, $x^{(k)}$ denotes the center of cell k and x_i represents a neighboring measurement cell. The Euclidean distance $\left|x_i - x^{(k)}\right|$ is the distance difference between cell k and the location of the measurement cell, which is always a positive value. The kernel width, σ plays an important parameter that determines the amount of extrapolation of the importance of measurement, r_i. Then, the confidence map, $\alpha^{(k)}$ will be introduced for the level of estimation of every cell k and computed as in Equation (3).

$$\alpha^{(k)} = 1 - e^{-\left(\Omega^{(k)}\right)^2/\sigma_\Omega^2} \quad (3)$$

The confidence map value, $\alpha^{(k),}$ is normalized and has a value in the interval of (1,0) with a scaling parameter, σ_Ω. Then, it will be used to compute the predictive mean at the respective cell, $r^{(k),}$ as in Equation (4).

$$r^{(k)} = \alpha^{(k)} \frac{R^{(k)}}{\Omega^{(k)}} + \{1 - \alpha^{(k)}\}.r_0 \quad (4)$$

The predictive mean is influenced by the confidence level, where a higher confidence level leads to the estimation approaching the weighted mean, $\frac{R^{(k)}}{\Omega^{(k)}}$. Conversely, with a lower confidence level, the mean estimation approaches to r_0 (i.e. the average overall sensor reading).

Then, the cumulative weight variance, $V^{(k)}$ of the gas measurement is calculated as in Equation (5).

$$V^{(k)} = \sum_{i=1}^{n} N\left(\left|x_i - x^{(k)}\right|, \sigma\right).(r_i - r^{(k(i))})^2 \quad (5)$$

where $k(i)$ is the nearby cell close to the measurement point, which is x_i and therefore $r^{(k(i))}$ refers to the predictive mean of cell k. Note that, Equation (5) is quite similar to Equation (2), except that the r_i is replaced by $(r_i - r^{(k(i))})^2$ to measure the variability of the reading with respect to the calculated mean. Lastly, the Predictive variance map is computed as in Equation (6).

$$v^{(k)} = \alpha^{(k)} \frac{V^{(k)}}{\Omega^{(k)}} + \{1 - \alpha^{(k)}\}.v_0 \quad (6)$$

A higher value of $\alpha^{(k)}$ converges toward $\frac{V^{(k)}}{\Omega^{(k)}}$, while lower value of $\alpha^{(k)}$ converge to v_0 (i.e. the average overall variance computation). This algorithm measures the variability of the gas reading with respect to the mean each time a new reading is acquired.

Temperature-Compensated Kernel DM+V Algorithm

The original algorithm of Kernel DM+V does not account for the surrounding conditions of an indoor environment. As noted in the literature, gas dispersion can

©2006-2026 Asian Research Publishing Network (ARPN). All rights reserved.

be affected by factors such as wind, ambient temperature, pressure, and obstacles. Incorporating these environmental conditions is therefore essential, particularly ambient temperature, which has not yet been integrated into the original algorithm.

This study proposes a Temperature-Compensated Kernel DM+V, where ambient temperature information is used to adjust the Gaussian kernel width, σ for gas reading extrapolation. By correlating the kernel width with ambient temperature measurements, the information content of the gas map will vary according to ambient temperature levels. As illustrated in Figure-5, smaller values of σ produce narrower bell-shaped kernels with minimal extrapolation, while larger σ values yield broader kernels, allowing greater extrapolation of sensor readings.

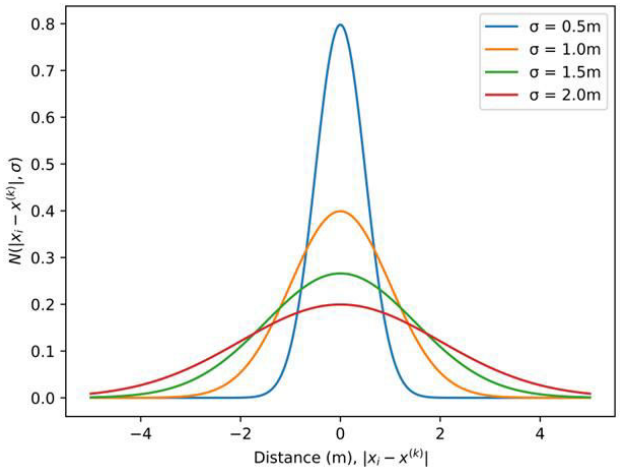


Figure-5. 1D Gaussian with variable kernel width, σ.

The formulation of Temperature-compensated Kernel DM+V is based on the cumulative important weight, $\Omega^{(k)}$, the cumulative weight reading $R^{(k)}$ and the cumulative weight variance, $V^{(k)}$ of original Kernel DM+V as shown in Equations (1), (2) and (5). These equations are modified to incorporate the Temperature-compensated kernel width, σ_T as presented in Equations (7)-(9). This algorithm assumes a linear dependency of the kernel width, which dynamically changes in response to varying ambient temperature readings.

$$\Omega^{(k)}(\sigma_T) = \sum_{i=1}^{n} N\left(\left|x_i - x^{(k)}\right|, \sigma_T\right), \quad (7)$$

$$R^{(k)}(\sigma_T) = \sum_{i=1}^{n} N\left(\left|x_i - x^{(k)}\right|, \sigma_T\right).r_i \quad (8)$$

$$V^{(k)}(\sigma_T) = \sum_{i=1}^{n} N\left(\left|x_i - x^{(k)}\right|, \sigma_T\right).(r_i - r^{(k(i))})^2 \quad (9)$$

Then, from the Equation (7), the Temperature-compensated confidence map is computed as Equation (10):

$$\alpha^{(k)}(\sigma_T) = 1 - e^{-\left(\Omega^{(k)}(\sigma_T)\right)^2/\sigma_\Omega^2} \quad (10)$$

Finally, the Temperature-compensated predictive mean map and variance map were obtained using Equation (11) and Equation (12) respectively.

$$r^{(k)}(\sigma_T) = \alpha^{(k)}(\sigma_T)\frac{R^{(k)}(\sigma_T)}{\Omega^{(k)}(\sigma_T)} + \{1 - \alpha^{(k)}(\sigma_T)\}.r_0 \quad (11)$$

$$v^{(k)}(\sigma_T) = \alpha^{(k)}(\sigma_T)\frac{V^{(k)}(\sigma_T)}{\Omega^{(k)}(\sigma_T)} + \{1 - \alpha^{(k)}(\sigma_T)\}.v_0 \quad (12)$$

The Temperature-compensated kernel width, σ_T depends on five parameters: the minimum threshold of kernel width, σ_{Min}, the maximum threshold of kernel width, σ_{Max}, the minimum threshold of ambient temperature, T_{Min}, the maximum threshold of ambient temperature, T_{Max}, and ambient temperature sensor readings, T_R. All parameters, except the ambient temperature sensor reading were determined heuristically.

The ambient temperature range has been set in the range of T_{Min} = 278.15 K (i.e. 5 °C) to T_{Max} = 313.15 K (i.e. 40 °C), representing most possible real-world indoor conditions. The kernel width size has been constrained within the interval of σ_{Min} = 0.5 m to σ_{Max} = 1.5 m since it is seen to produce a more correct map prediction. They emphasize the importance of avoiding excessively narrow or wide kernel widths. A narrow width leads to under-smoothing in the GDM, whereas an excessively wide width results in over-smoothing [24].
The value of Temperature-compensated kernel width, σ_T is determined as shown in Equation (13):

$$\sigma_T = \begin{cases} \sigma_{Max} & : \quad T_R > T_{Max} \\ \sigma_0 + \sigma_{Min} & : \quad T_{Min} \leq T_R \leq T_{Max} \\ \sigma_{Min} & : \quad T_R < T_{Min} \end{cases} \quad (13)$$

where the value of σ_T is determined based on ambient temperature readings, T_R. If T_R exceeds the maximum threshold, T_{Max}, or less than the minimum threshold, T_{Min}, the value of σ_T is set to the maximum, σ_{Max} or minimum, σ_{Min} respectively. However, if the, T_R lies within the range of minimum and maximum threshold of ambient temperature, σ_T is calculated as the sum of the kernel node, σ_0 and minimum value of kernel width, σ_{Min}. Equation (14) presents the derivation used to obtain the kernel node, σ_0.

$$\sigma_0 = \frac{\sigma_{Max} - \sigma_{Min}}{T_{Max} - T_{Min}}(T_R - T_{min}) \quad (14)$$

It should be noted that this algorithm is suitable only for indoor environments, where the effect of wind is minimal. Applying it outdoors could lead to incorrect interpretations of gas dispersion, as strong wind can significantly alter the spread of gas. Figure-6 illustrates an example of varying extrapolation sizes of kernel widths at different ambient temperature levels (i.e. cool and warm conditions) for both original and proposed GDM methods. In the original method, the kernel width remains consistent, regardless of changes in environmental

©2006-2026 Asian Research Publishing Network (ARPN). All rights reserved.

conditions during mobile robot exploration. In contrast, the proposed method dynamically adjusts the kernel width in response to the surrounding environmental conditions.

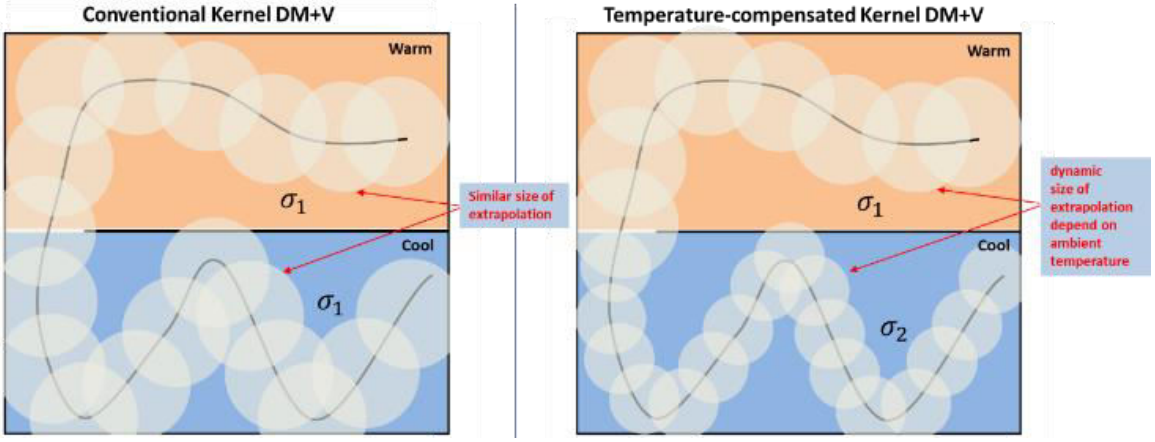


Figure-6. Example of varying extrapolation sizes at different ambient temperature levels for the conventional and Temperature-compensated GDM methods.

Mobile Robot Architecture

The Bveeta Mini Type R robot was used in this study to collect the data required for the experiments. Figure-7 shows all the robot's components and its label.

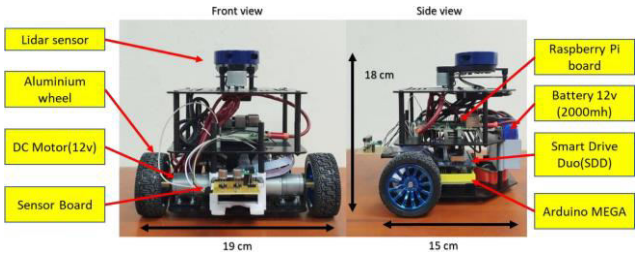


Figure-7. Bveeta robot.

The robot comes with a dimension of 18 cm (height) x 19 cm (width) x 15 cm (length), with the size of the robot's aluminum wheel 6 cm in diameter respectively. Both wheels are attached to the 12 V Direct Current (DC) motor with the encoder which is controlled via the Smart Drive Duo (SDD) board and each of the DC motor can reach up to 130 rpm. However, the robot was operated at a maximum speed of 5 cm/s during the data collection process since this speed had been commonly employed by prior researchers to facilitate interaction between the gas sensor and the released gas [8]. A 12 V battery with a capacity of 2000 mAh was used to supply power to all robot's components, enabling the robot to operate with a maximum time of 2.5 hours continuously. The Raspberry Pi 4 Model B is the main component of the robot and acts as a mini computer installed with the Ubuntu 18.04 operating system. The ROS master runs on this microcomputer and oversees all the ROS nodes from both the base station and the robot system. The Raspberry Pi communicates with the Arduino MEGA via the ROS bridge tool, which allows the Arduino board to acquire sensor readings (e.g. from the sensor board and motor encoder) and publish them to the Raspberry Pi. The robot has been equipped with a sensor board to collect important information in the contaminated area, especially information on gas and ambient temperature. Figure-8 shows the customized sensor board installed on the robot.

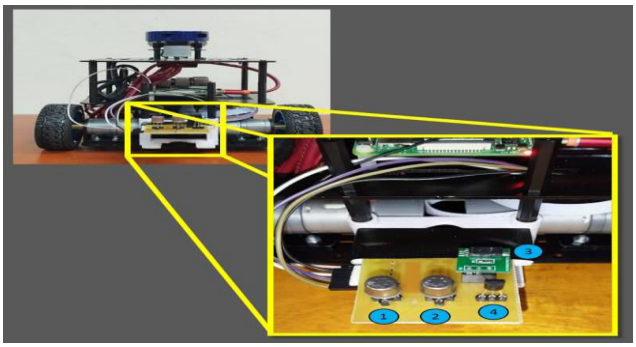


Figure-8. Sensor board installed on the robot: (1) MOX 1, (2) MOX 2, (3) humidity, and (4) temperature sensor.

The main function of the sensor board is to measure the important information of the contaminated area such as gas concentration, temperature, and percentage of relative humidity reading. The sensor board was equipped with two Figaro TGS 2600 gas sensors (sensor 1 and sensor 2) to measure the VOCs concentration reading, while ambient temperature and relative humidity were measured by using a typical LM35 (sensor 4) and HIH-5030 (sensor 3) respectively. The sensor board was positioned at the front of the robot, 5 cm above ground level, as front-mounted configurations are widely adopted in GSL applications [27]. This placement is also appropriate because the ethanol used in this study is denser than ambient air and tends to disperse near the ground. In addition, the sensor board was directly exposed to the environment rather than put inside a chamber with a fan as implemented in the work [28-31]. This design could

©2006-2026 Asian Research Publishing Network (ARPN). All rights reserved.

minimize the risk of altering the concentration, temperature, humidity, and surrounding airflow that could occur in a controlled chamber environment.

Experimental Setup

An experiment was conducted to investigate the effects of cool and warm ambient temperature levels on the proposed GDM method within a cabin room located at the Faculty of Electrical Engineering & Technology, Universiti Malaysia Perlis. The cabin room has dimensions of 12 m (length) x 7 m (width) x 3 m (height). It is equipped with five wall-mounted air-conditioning units, each with a capacity of 2.5 hp, which can be activated to cool the room as needed. Notably, the ambient temperature within the cabin is influenced by external weather conditions. On sunny days, when outdoor temperatures are high, the ambient temperature inside the room can rise to a maximum of 40 °C in the absence of air-conditioning. Conversely, during the night, the ambient temperature can drop to approximately 18 °C when the air-conditioning units are in operation.

Five distinct and random locations were carefully selected to represent a diverse range of scenarios. For each of these locations, gas release experiments were conducted under two specific ambient temperature conditions: cool and warm environments. The spatial arrangement of the gas sources within the room is illustrated in Figure-9, while Table-1 provides precise coordinates of each gas source location.

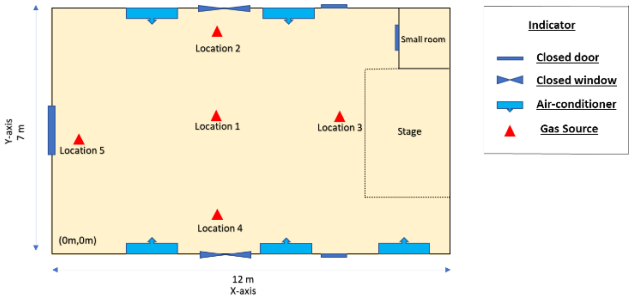


Figure-9. Five different locations of gas sources inside the cabin room.

Table-1. Different locations of the gas source.

Location	Coordinate (m)	
	X	Y
1	4.32	3.44
2	4.32	5.63
3	8.13	3.75
4	4.32	0.91
5	0.71	2.78

For the purpose of this study, the gas source was simulated using a container filled with a 95% ethanol solution, which served as a representative medium for the harmful gas released during the experiments. When the gas is released, an increase in concentration in the local surroundings of the source will be an immediate result. Fluid dynamic effects like advection (wind) or diffusion may then carry the increased concentration further into the environment [32]. To maintain controlled experimental conditions, all air gaps in the experimental room were effectively sealed to prevent disturbances caused by strong airflow that could influence the dispersion of the released gas. Additionally, all windows and doors were closed during the experiments, ensuring that gas distribution remained unaffected by external factors.

In order to create distinct environmental conditions for the experiment, specific measures were taken. For the warm environment, the experimental trials were conducted during the afternoon on a sunny day, without any air-conditioning units being activated. This approach ensured that the room was maintained at a warm temperature. Conversely, for the cool environment, the experiments were conducted at midnight, taking advantage of the lower outdoor temperature. This step helped to minimize the heat transfer process and facilitated easier control of the cool temperature within the room.

To establish a cool environment, all five air-conditioning units were activated and set to a temperature of 16 °C for a duration of three hours, effectively cooling the ambient temperature within the room. However, prior to commencing the experiment, all air-conditioning units were turned off to prevent significant airflow, thus allowing for the natural dispersion of the gas after exposure.

After five minutes of gas exposure, a mobile robot equipped with sensors was deployed and controlled by the operator to collect data measurements. The robot followed a predefined trajectory at a maximum speed of 5 cm/s in a deliberate sweeping pattern within the designated area, as depicted in Figure-10. This systematic movement strategy ensured comprehensive data collection across the entire spatial domain while simultaneously recording real-time ambient temperature readings and mapping the structure of the building. All procedures were repeated for each of the five distinct locations mentioned previously, enabling the acquisition of data from various gas sources under different environmental conditions.

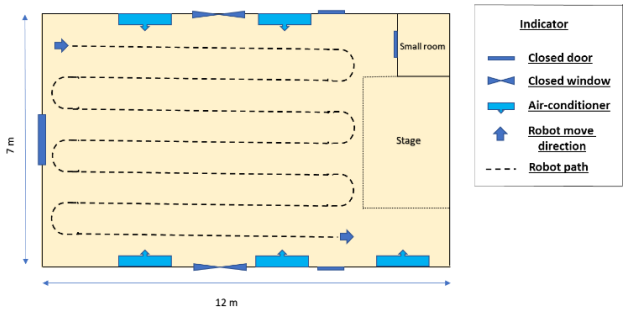


Figure-10. Robot path inside the cabin room for data collection with manual control.

©2006-2026 Asian Research Publishing Network (ARPN). All rights reserved.

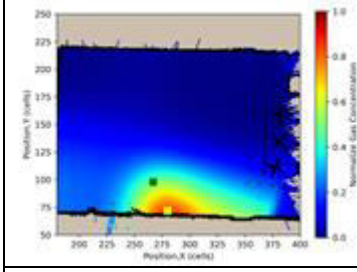
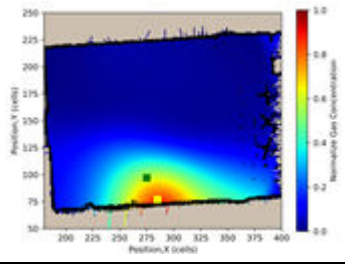
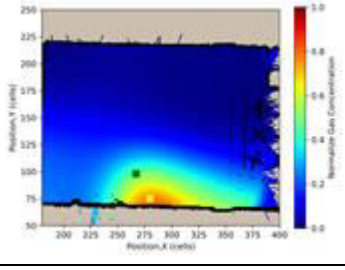
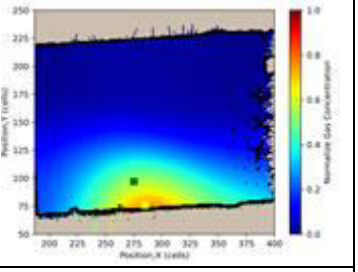
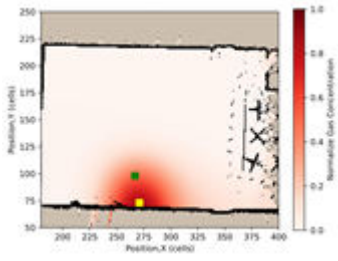
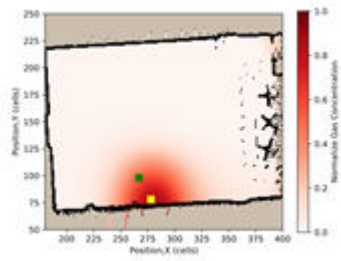
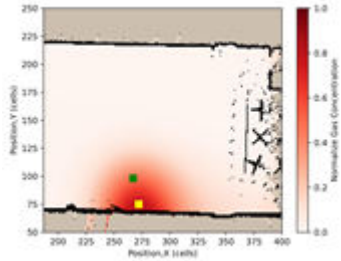
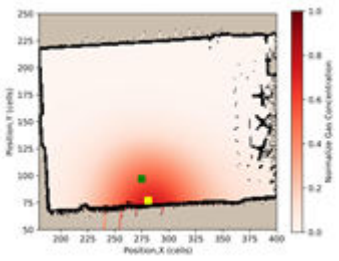
RESULTS AND DISCUSSIONS

This section will discuss the experimental results of GDM collected under different ambient temperatures in both qualitative and quantitative aspects, highlighting the difference in map representation and gas localization accuracy.

Qualitative Results of GDM

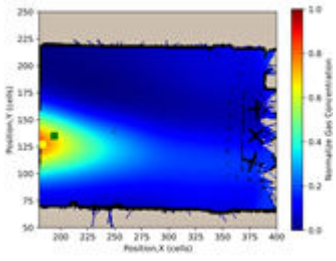
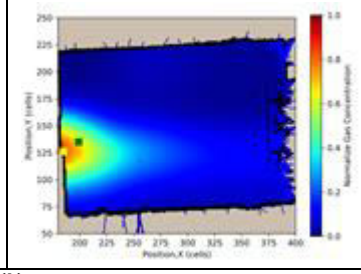
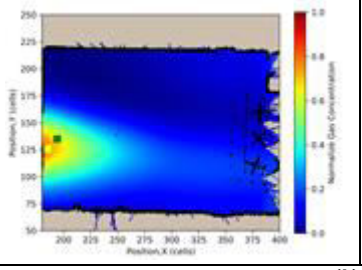
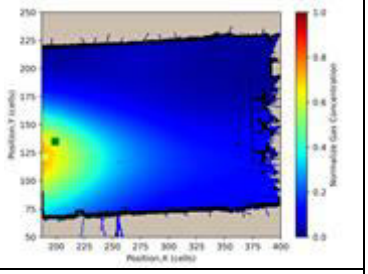
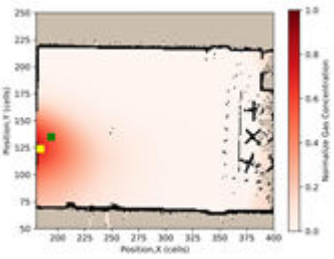
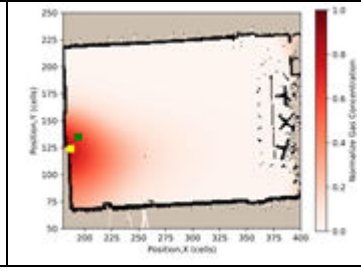
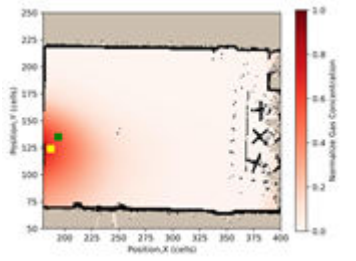
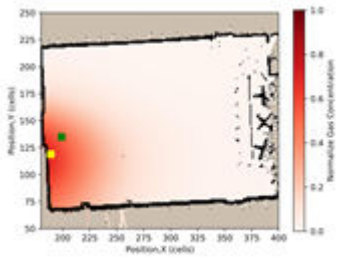
Table-2 and Table-3 present the predictive mean and predictive variance maps for Gas Location 5 and 4 under different ambient temperature conditions (cool and warm), using two methods: Kernel DM+V and Temperature-compensated Kernel DM+V. In the predictive mean maps, gas concentration is visualized using the 'Jet' color scale, where higher concentrations of gas appear as intense red regions and lower concentrations as intense blue regions. In contrast, the predictive variance maps use the 'Reds' color scale. Areas with higher variance are shown in deeper red tones, whereas lighter red tones indicate lower variance. The Black regions in all maps denote walls and obstacles encountered along the robot's trajectory. Furthermore, each gas map is plotted with the actual and predicted locations of the gas source, where the green square indicates the actual gas source, and the yellow square marks the location predicted by the global maximum.

Table-2. Gas distribution map result at location 4.

Kernel DM+V		**Temperature-compensated Kernel DM+V**	
$r^{(k)}$		$r^{(k)}(\sigma_T)$	
Cool	Warm	Cool	Warm
			
$v^{(k)}$		$v^{(k)}(\sigma_T)$	
Cool	Warm	Cool	Warm
			
Global maximum		Actual location	

©2006-2026 Asian Research Publishing Network (ARPN). All rights reserved.

Table-3. Gas distribution map result at location 4.

Kernel DM+V		**Temperature-compensated Kernel DM+V**	
$r^{(k)}$		$r^{(k)}(\sigma_T)$	
Cool	Warm	Cool	Warm
			
$v^{(k)}$		$v^{(k)}(\sigma_T)$	
Cool	Warm	Cool	Warm
			
Global maximum		Actual location	

The table highlights the differences between methods that incorporate ambient temperature information and those that do not. When ambient temperature is considered, the algorithm dynamically adjusts the kernel width in response to environmental conditions. For example, in warmer environments, gas molecules gain kinetic energy, leading to increased movement and broader dispersion. This causes the gas concentration to spread over a wider area, which the algorithm compensates for by expanding the kernel width. Consequently, the model can more accurately reflect the larger dispersion area. Conversely, in cooler environments, where gas molecules exhibit less kinetic energy and remain more concentrated, a narrower kernel width is used to match the smaller dispersion area.

In cases where ambient temperature is not considered, the model uses a fixed kernel width, regardless of temperature variations. This approach may perform adequately in stable or moderate conditions, but it can lead to errors when applied to highly variable environments. For instance, in warm conditions, the fixed kernel width may not fully capture the extent of gas dispersion, potentially leading to an underestimation of the affected area. On the other hand, in cooler conditions, a fixed kernel width might overestimate dispersion.

For gas source localization, the global maximum value in each gas map is used as the estimated source position. Based on the observations, most predicted locations fall within regions of high concentration, as the global-maximum approach naturally identifies highly concentrated cells as emission points. However, these high-concentration regions often accumulate near walls, which contributes to increased localization error. Overall, both methods yield similar predictions for the gas source location.

Quantitative Results of GDM

Qualitative observations indicate that gas distribution maps generated under warmer ambient conditions present a noticeably broader spread of gas concentration compared to those produced in cooler environments. This finding is further evaluated through quantitative analysis, comparing the fluctuating percentage changes in total white pixel values under both conditions. Table-4 presents a comprehensive summary of the white pixel readings for each gas map, considering the ambient temperature information, as well as a separate analysis without taking ambient temperature into account.

©2006-2026 Asian Research Publishing Network (ARPN). All rights reserved.

Table-4. Summary of pixel binary number 1 (cell value > 0.9).

Gas location	Ambient condition	With ambient temperature consideration				Without ambient temperature consideration			
		Mean Map		Var Map		Mean Map		Var Map	
Loc. 1	cool	1948	+131%	1049	+72%	1639	+78%	892	-8%
	warm	4505		1806		2925		820	
Loc. 2	cool	491	+71%	561	+179%	486	+10%	748	+23%
	warm	840		1566		535		918	
Loc. 3	cool	1151	+48%	911	+129%	1037	+8%	604	+19%
	warm	1709		2088		1119		718	
Loc. 4	cool	1052	+31%	684	+33%	1010	+8%	460	+8%
	warm	1377		909		1090		496	
Loc. 5	cool	537	+46%	408	+79%	431	-13%	316	-10%
	warm	784		730		376		349	

According to the table, when there is no ambient temperature consideration, the mean map and variance map for all locations exhibit a minor difference in gas spread, despite being released at different ambient levels. For example, the difference in gas concentration for the mean map in “Location 3” and “Location 4” exhibits only +8% from a cool to a warm environment. In the worst case by neglecting ambient temperature information, the mean map and variance map in “Location 5” exhibit -13% and -10% of concentration changing even though the environment changes from cool to warm. This oversight can lead to misinterpretations of the actual gas dispersion behavior in real-world conditions, where gas in warmer environments would typically spread over a broader area compared to cooler environments. In general, most GDMs without ambient temperature consideration show insignificant and inconsistent percentage changes of gas concentration in cool and warm environments which do not reflect the environment condition.

Conversely, by taking the ambient temperature into consideration, significant and consistent percentage changes are observed across most GDMs for both cool and warm environments. Each GDM result demonstrates a positive, consistent increase in gas spread from cool to warm conditions, aligning with the expected behavior of gas dispersion in real-world settings. This indicates that the proposed algorithm effectively adjusts gas spread in response to specific environmental conditions, without requiring manual adjustments to the kernel width. This adaptability enables operators or rescuers to identify high-risk areas accurately, thereby enhancing their capacity to respond swiftly and efficiently to mitigate the hazards of harmful gas exposure.

Figure-11 illustrates the result in Table-4 for better visual interpretation. From the histogram chart, it can be seen that the GDM algorithm with ambient temperature considerations produces more consistently wider gas dispersion under warmer conditions. In contrast, the GDM algorithm without ambient temperature consideration shows a noticeably smaller increase in dispersion from cool to warm environments, and in some locations even a reduction. This behavior does not accurately reflect the fundamental principles of gas law, where higher ambient temperatures are expected to enhance gas diffusion and spread.

©2006-2026 Asian Research Publishing Network (ARPN). All rights reserved.

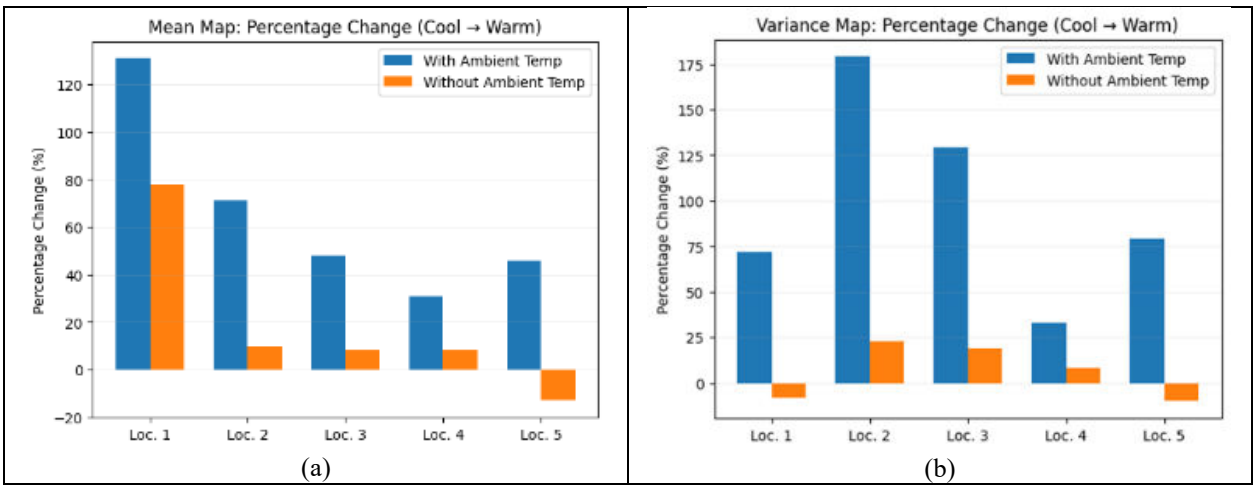


Figure-11. Summary of pixel binary number 1 (cell value > 0.9) for (a) Mean map and (b) Variance map.

Table-5 provides a comprehensive quantitative evaluation of the Euclidean distance errors between actual and predicted gas source locations for both the predictive mean and variance maps across five specific locations under two ambient conditions (i.e., cool and warm). This table offers valuable insights into the accuracy of the gas maps for each location under varying ambient temperature settings.

Table-5. Euclidean distance error between the actual and predicted gas source location.

	Map	Ambient condition	Euclidean distance Error (m)					Average Error (m)
			Loc. 1	Loc. 2	Loc. 3	Loc. 4	Loc. 5	
With ambient temperature consideration	Mean Map	Cold	1.78	1.53	2.27	1.32	0.64	1.51
		Warm	1.51	1.50	2.34	1.16	0.83	1.47
	Var Map	Cold	1.13	1.41	2.33	1.18	1.04	1.42
		Warm	0.57	1.44	1.80	1.04	0.94	1.16
without ambient temperature consideration	Mean Map	Cold	1.75	1.50	2.07	1.45	0.68	1.49
		Warm	1.15	1.50	1.95	1.12	0.83	1.31
	Var Map	Cold	1.17	1.40	2.23	1.27	0.74	1.36
		Warm	0.61	1.03	1.30	0.96	0.81	0.94

From the table, it can be observed that cool and warm conditions have minimal impact on the accuracy of gas localization, with distances ranging from 0.57 m to 2.34 m. The average distance error between the actual and predicted gas source locations was between 1.16 m to 1.51 m. This variance is attributed to predictions in "Location 3," which show the largest distance error, as most of the gas concentration accumulates along the building's wall, contributing to the overall increase in average distance error. However, the distance error observed in this experiment remains within an acceptable range, given the extensive size of the test area. Figure-12 shows the summary result from Table-5.

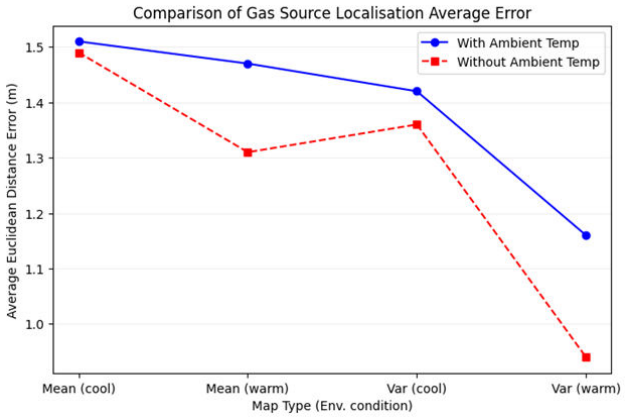


Figure-12. Average Euclidean distance error for gas localization.

©2006-2026 Asian Research Publishing Network (ARPN). All rights reserved.

For the predictive mean map and variance map, without considering ambient temperature in both cool and warm environments, three out of five gas location predictions are more accurate compared to those maps that incorporate ambient temperature. However, the error rates for both methods are comparable, with differences not particularly pronounced. Overall, the average prediction error for gas source localization for the GDM without ambient temperature consideration is lower compared to the GDM that accounts for ambient temperature.

The reason for this is that when ambient temperature is taken into account, the GDM dynamically increases the kernel width in warm environments to accommodate the broader gas spread. While this theoretically aligns with the larger dispersion, it can also decrease localization accuracy. A larger kernel width smooths the concentration gradient, reducing the model's sensitivity to subtle concentration variations near the source. This may result in the predicted gas source position being less precise, as the larger kernel size effectively 'averages out' nearby concentration peaks that could otherwise help pinpoint the origin more accurately. Thus, instead of sharply focusing on a localized peak, the model spreads the effect over a larger area, making it challenging to locate the true source.

Unlike models incorporating ambient temperature, the GDM with a fixed kernel width does not adjust for environmental changes. This narrower kernel results in a concentrated distribution that accentuates high concentration areas near the source, even in warmer conditions. Consequently, the model's predictions may more accurately reflect the actual gas source location, as it consistently applies uniform spatial parameters for localization regardless of varying environmental factors.

CONCLUSIONS

As most existing studies on Gas Distribution Mapping (GDM) often overlook the influence of ambient temperature on gas dispersion in indoor environments, this study demonstrates an improved version of Kernel DM+V by incorporating ambient temperature information. The improved algorithm, known as the Temperature-compensated Kernel DM+V, was successfully developed and tested in the controlled indoor environment under both cool and warm conditions. Experimental results show that the proposed algorithm could produce more realistic and spatially consistent gas distribution estimations, particularly in areas affected by ambient temperature differences. The algorithm allowed the system to adjust its Gaussian convolution based on temperature, producing a more realistic gas distribution map and preventing the misinterpretation of gas behavior under varying thermal conditions. However, the integration of ambient temperature reduces sensitivity to kernel width and the robustness of source localization predictions, as the larger kernel size effectively 'averages out' nearby concentration peaks that could otherwise help pinpoint the origin more accurately. Thus, instead of sharply focusing on a localized peak, the model spreads the effect over a larger area, making it challenging to locate the true source. Overall, the findings confirm that ambient temperature is a critical factor in indoor gas dispersion. Incorporating temperature information into the Kernel DM+V framework substantially enhances the realism and practical reliability of GDM, supporting its adoption in real-world indoor monitoring and mobile robot olfaction applications.

ACKNOWLEDGEMENT

The authors would like to acknowledge the support from the Fundamental Research Grant Scheme (FRGS) under a grant number of FRGS/1/2018/ICT05/UNIMAP/02/4 from the Ministry of Education Malaysia.

REFERENCES

[1] The Sun Daily. 2020. Ammonia gas leak: 59 factory workers fall sick in Kulim. The Sun Daily, [Online]. Available: https://www.thesundaily.my/local/ammonia-gas-leak-59-factory-workers-fall-sick-in-kulim-XC1958404

[2] New Straits Times. 2023. Gas leak kills 11 people in India. New Straits Times, [Online]. Available: https://www.nst.com.my/world/world/2023/04/904369/gas-leak-kills-11-india

[3] M. Kang, J. Son, B. Lee and H. Nam. 2024. Reconstruction of the chemical gas concentration distribution using partial convolution-based image inpainting. Sensors. 24(14).

[4] M. A. Arain, V. H. Bennetts, E. Schaffernicht and A. J. Lilienthal. 2021. Sniffing out fugitive methane emissions: Autonomous remote gas inspection with a mobile robot. The International Journal of Robotics Research. 40(4-5): 782-814.

[5] H. H. Erwich, B. P. Duisterhof and G. C. H. E. de Croon. 2024. GSL-Bench: High-fidelity gas source localization benchmarking tool. In Proceedings of the 2024 IEEE International Conference on Robotics and Automation, Yokohama, Japan. pp. 17672-17678.

[6] Y. Yang, J. Liu, W. Wang, Y. Cao and H. Li. 2021. Incorporating SLAM and mobile sensing for indoor carbon dioxide monitoring and source position estimation. Journal of Cleaner Production. 291(Art. no. 125780).

[7] N. Evalina and H. A. Azis. 2020. Implementation and design of a gas leakage detection system using an

©2006-2026 Asian Research Publishing Network (ARPN). All rights reserved.

ATMega8 microcontroller. IOP Conference Series: Materials Science and Engineering. 821(1): Art. no. 012049.

[8] A. J. Lilienthal, M. Reggente, M. Trincavelli, J. L. Blanco and J. Gonzalez. 2009. A statistical approach to gas distribution modelling with mobile robots: The Kernel DM+V algorithm. In Proceedings of the 2009 IEEE/RSJ International Conference on Intelligent Robots and Systems, St. Louis, MO, USA. pp. 570-576.

[9] V. H. Bennetts, E. Schaffernicht, V. Pomareda, A. J. Lilienthal, S. Marco and M. Trincavelli. 2014. Combining non-selective gas sensors on a mobile robot for identification and mapping of multiple chemical compounds. Sensors. 14(9): 17331-17352.

[10] J. Yang *et al*. 2024. A multi-UAV indoor air real-time detection and gas source localization method based on improved teaching–learning-based optimization. Atmospheric Environment. 318(Art. no. 120200).

[11] Z. H. M. Juffry, K. Kamarudin, A. H. Adom, M. F. Miskon and A. N. Abdullah. 2023. Theoretical and numerical study on the effect of ambient temperature on gas dispersion in an indoor environment using a computational fluid dynamics approach. Journal of Advanced Research in Fluid Mechanics and Thermal Sciences. 105: 194-209.

[12] A. T. Hayes, A. Martinoli and R. M. Goodman. 2002. Distributed odor source localization. IEEE Sensors Journal. 2(3): 260-271.

[13] J. Lilienthal, H. Ulmer and A. Zell. 2004. Building gas concentration gridmaps with a mobile robot. Robotics and Autonomous Systems, 48(1): 3016, doi: 10.1016/j.robot.2004.05.002.

[14] M. Reggente and A. J. Lilienthal. 2009. Three-dimensional statistical gas distribution mapping in an uncontrolled indoor environment. AIP Conference Proceedings. 1137: 109-112.

[15] A. J. Lilienthal, A. Loutfi, J. L. Blanco, C. Galindo and J. Gonzalez-Jimenez. 2014. A Rao-Blackwellisation approach to GDM-SLAM: Integrating simultaneous localisation and mapping and gas distribution mapping. In Proceedings of the European Conference on Mobile Robots, Barcelona, Spain. pp. 126-131.

[16] B. Stachniss, C. Plagemann, A. Lilienthal and W. Burgard. 2009. Gas distribution modeling using sparse Gaussian process mixture models. In Proceedings of Robotics: Science and Systems, Seattle, WA, USA. pp. 310-317.

[17] M. Reggente and A. J. Lilienthal. 2009. Using local wind information for gas distribution mapping in outdoor environments with a mobile robot. in Proceedings of the 2009 IEEE Sensors Conference, Christchurch, New Zealand. pp. 1715-1720, doi: 10.1109/ICSENS.2009.5398498.

[18] M. Reggente and A. J. Lilienthal. 2010. The 3D Kernel DM+V/W algorithm: Using wind information in three-dimensional gas distribution modelling with a mobile robot. In Proceedings of the IEEE Sensors Conference, Kona, HI, USA. pp. 999-1004.

[19] P. Neumann, Gas Source Localization and Gas Distribution Mapping with a Micro-Drone, Berlin, Germany: Federal Institute for Materials Research and Testing, 2013.

[20] W. Jin and A. Martinoli. 2024. Sense in motion with belief clustering: Efficient gas source localization with mobile robots. in Proceedings of the IEEE International Conference on Robotics and Automation, Yokohama, Japan. pp. 14909-14916.

[21] A. Francis, S. Li, C. Griffiths and J. Sienz. 2022. Gas source localization and mapping with mobile robots: A review. Journal of Field Robotics. pp. 1341-1373.

[22] D. Li *et al*. 2024. Advanced Kernel DM+V/W+ method for precise mapping of pollutant dispersion in indoor environments. Journal of Cleaner Production. 480(Art. no. 144101).

[23] J. G. Monroy, J. L. Blanco y J. González-Jiménez. 2016. Time-variant gas distribution mapping with obstacle information. Autonomous Robots. 40(1): 1-16.

[24] K. Kamarudin. 2016. An improved mobile robot-based gas source localization with temperature and humidity compensation via SLAM and gas distribution mapping. Ph.D. dissertation, Universiti Malaysia Perlis, Malaysia.

[25] K. Kamarudin *et al*. 2018. Integrating simultaneous localisation and mapping and gas distribution

©2006-2026 Asian Research Publishing Network (ARPN). All rights reserved.

mapping for real-time gas source localization. Advanced Robotics. 32(17): 903-917.

[26] R. Visvanathan *et al*. 2020. Improved mobile robot-based gas distribution mapping through propagated distance transform for structured indoor environments. Advanced Robotics. 34(10): 637-647.

[27] Y. Zhai and Y. Miao. 2024. Gas-source efficient active searching in unfamiliar environments. In Proceedings of the 2024 IEEE International Conference on Robotics and Automation, Yokohama, Japan. pp. 18384-18390.

[28] L. L. López *et al*. 2011. Moth-like chemo-source localization and classification on an indoor autonomous robot. IntechOpen.

[29] A. Murai *et al*. 2015. Robotic gas source localization assisted by active airflow generation. In Proceedings of the IEEE Sensors Conference, Busan, South Korea. pp. 1-4.

[30] T. Wiedemann, D. Shutin and A. J. Lilienthal. 2019. Model-based gas source localization strategy for a cooperative multi-robot system: A probabilistic approach and experimental validation. Robotics and Autonomous Systems. 118: 66-79.

[31] Y. Yang *et al*. 2019. Experimental study on single-robot active olfaction algorithms for locating contaminant sources in indoor environments without strong airflow. Building and Environment. 155: 320-333.

[32] P. Hinsen, T. Wiedemann, D. Shutin and A. J. Lilienthal. 2023. Exploration and gas source localization in advection-diffusion processes with potential-field-controlled robotic swarms. Sensors. 23(22).

[33] Hérès X., *et al*. 2018. Selective extraction of rare earth elements from phosphoric acid by ion exchange resins. Metals. 8(9): 682.